Kinetics and identities of extracellular peptidases in subsurface sediments of the White Oak River Estuary, NC

Running title: Extracellular enzymes in subsurface sediments

Andrew D. Steen[a,#], Richard T. Kevorkian[b], Jordan T. Bird[b], Nina Dombrowski[c], Brett J. Baker[c], Shane M. Hagen[a], Katherine H. Mulligan[a,d], Jenna M. Schmidt[a], Austen T. Webber[a], Marc J. Alperin[e]

[a]Department of Earth and Planetary Sciences, University of Tennessee, Knoxville, Tennessee, USA

[b]Department of Microbiology, University of Tennessee, Knoxville, Tennessee, USA

[c]Department of Marine Science, University of Texas-Austin, Marine Science Institute, Port Aransas, Texas, USA

[d]Department of Biology, University of North Carolina at Chapel Hill, Knoxville, Tennessee, USA

[e]Department of Marine Sciences, University of North Carolina at Chapel Hill, USA

[#]Corresponding author. email: asteen1@utk.edu

mail: Strong Hall 601, 1621 Cumberland Avenue, Knoxville, TN 37996-1410

tel: (865) 974-4014, fax: (865) 974 2638

Abstract

Anoxic subsurface sediments contain communities of heterotrophic microorganisms that oxidize organic carbon at extraordinarily slow rates. In order to assess the mechanisms by which subsurface microorganisms access detrital sedimentary organic matter, we measured kinetics of a range of extracellular peptidases in anoxic sediments of the White Oak River estuary, NC. Nine distinct peptidase substrates were enzymatically hydrolyzed at all depths. Potential peptidase activities (V_{max}) decreased with increasing sediment depth, although V_{max} expressed on a per cell basis was approximately the same at all depths. Half-saturation constants (K_m) decreased with depth, indicating that subsurface enzymes are adapted to low substrate concentrations. Potential activities of extracellular peptidases acting on molecules that are enriched in degraded organic matter (D-phenylalanine and L-ornithine) increased relative to enzymes that act on L-phenylalanine, further suggesting microbial community adaptation to access degraded organic matter. Nineteen classes of exported peptidases were identified in genomic data from the same site, of which genes for class C25 (gingipain-like) peptidases represented more than 40% at each depth. Methionine aminopeptidases, zinc carboxypeptidases, and class S24-like peptidases, which are involved in single-stranded DNA repair, were also abundant. These results suggest a subsurface heterotrophic microbial community that primarily accesses low-quality detrital organic matter via a diverse suite of well-adapted extracellular enzymes.

IMPORTANCE

Burial of organic carbon in marine and estuarine sediments represents a long-term sink for atmospheric carbon dioxide. Globally, ~40% of organic carbon burial occurs in anoxic estuaries and deltaic systems. However, the ultimate controls on the amount of organic matter that is buried in sediments, versus oxidized into CO_2, are poorly constrained. Here we used a combination of enzyme assays and metagenomic analysis to identify how subsurface microbial communities catalyze the first step of proteinaceous organic carbon degradation. Our results show that microbial communities in deeper sediments are adapted to access molecules characteristic of degraded organic matter, suggesting that those heterotrophs are adapted to life in the subsurface.

Introduction

A large fraction of the microorganisms in subsurface sediments are heterotrophs that metabolize aged, microbially altered organic matter (Lomstein *et al.*, 2009; Jørgensen and Marshall, 2016; Biddle *et al.*, 2006). These communities' metabolisms can be more than a million-fold more slower than cells in culture (Hoehler and Jørgensen, 2013; Lomstein *et al.*, 2009). A recent meta-analysis showed that only about 12% of cells in marine sediments belonged to cultured species, while 27% belong to phyla that contain no cultured representatives (Lloyd *et al.*, 2018). Consequently, the mechanisms by which these microorganisms access detrital organic matter are poorly understood.

In surface environments, where carbon transformations are relatively rapid, heterotrophic microorganisms gain energy by metabolizing a combination of small molecules (<600-1000 Da), which can be taken up directly via general uptake porins (Benz and Bauer, 1988) and macromolecules, which must be broken down outside of the cell by extracellular enzymes. Most freshly-produced organic matter is macromolecular, and large molecules tend to be more bioavailable than small ones (Benner and Amon, 2015), so the nature and activity of extracellular enzymes present in surface environments is a major control on the rate of microbial carbon oxidation in such environments.

It is not clear whether microbial extracellular enzymes play the same role in subsurface sediments. It is conceivable that macromolecules are broken down primarily by non-enzymatic mechanisms in sediments. For instance, in soils, MnO_4 catalyzes the depolymerization of proteins without requiring enzymes. Certain bacterial species can use TonB-dependant transporters to transport polysaccharides that are substantially larger

77 than 600 Da into the periplasm (although enzymatic hydrolysis is still required prior to
78 uptake into the cytoplasm; Reintjes *et al.*, 2017). Furthermore, some of the unique aspects
79 of subsurface sediments suggest that extracellular enzymes might not be an effective
80 strategy to obtain carbon or energy. In order for the production of extracellular enzymes
81 to be part of a viable metabolic strategy, each enzyme must, over its lifetime, provide the
82 cell with at least as much carbon or energy as was required to synthesize the enzyme
83 (Vetter *et al.*, 1998; Allison, 2005; Schimel and Weintraub, 2003). In subsurface
84 sediments, where cell division times may be on the order of decades to millenia, enzyme
85 lifetimes would need to be correspondingly longer to remain 'profitable'. Since enzyme
86 lifetimes are finite, there must exist a community metabolic rate below which
87 extracellular enzyme lifetimes are too short to become profitable. That limit is difficult to
88 quantify because enzyme lifetimes in any environment are poorly constrained (e.g., Steen
89 and Arnosti, 2011). Thus, it is plausible that extracellular enzyme-mediated carbon
90 acquisition is impractical in sediments in which metabolic rates are particularly slow.
91 While extracellular enzyme activity in surface sediments has frequently been
92 reported, few reports exist of extracellular enzyme activity from deeper than 20 cm below
93 the seafloor (cmbsf) (Arnosti *et al.*, 2014). Enzyme activity has been reported in
94 sapropels up to 389 cmbsf in sapropels in the Eastern Mediterranean Sea (Coolen and
95 Overmann, 2000; Coolen *et al.*, 2002) and in sediment from 600-630 cmbsf in Aarhus
96 Bay sediments (Lloyd *et al.*, 2013a), as well as in a few other subsurface environments,
97 such as the interior of seafloor basalts at the Loihi seamount (Jacobson Meyers *et al.*,
98 2014). Furthermore, an analysis of transcriptomes from subsurface sediments of the Peru

99 Margin revealed diverse exported peptidases and carbohydrate-active enzymes, which
100 decreased in relative abundance with increasing depth (Orsi *et al.*, 2018).
101 In order to better understand how heterotrophic microorganisms in subsurface
102 sediments access organic matter, we assayed a diverse set of peptidases (protein-
103 degrading enzymes) in sediment cores from the White Oak River estuary, NC. We paired
104 these assays with analysis of the potential for extracellular peptidase production from
105 existing metagenomic data sets. We chose this site because the porewater geochemistry
106 and microbiology of these sediments has been well-characterized (Martens and
107 Goldhaber, 1978; Kelley *et al.*, 1990; Baker *et al.*, 2015; Lazar *et al.*, 2016; Lloyd *et al.*,
108 2011) and because they contain abundant Bathyarchaeota and Thermoprofundales
109 archaea, which appear to be capable of metabolizing detrital organic matter (Kubo *et al.*,
110 2012; Lloyd *et al.*, 2013a; Meng *et al.*, 2014; Zhou *et al.*, 2018b). We focused on
111 peptidases because protein degradation appears to be an important metabolism for some
112 subsurface archaea (Lloyd *et al.*, 2013a) and because peptidases were more active than
113 other enzymes in similar environments (Coolen and Overmann, 2000; Jacobson Meyers
114 *et al.*, 2014). Because environmental samples contain a wide range of distinct peptidases
115 at variable activities (Obayashi and Suzuki, 2005; Steen and Arnosti, 2013) we measured

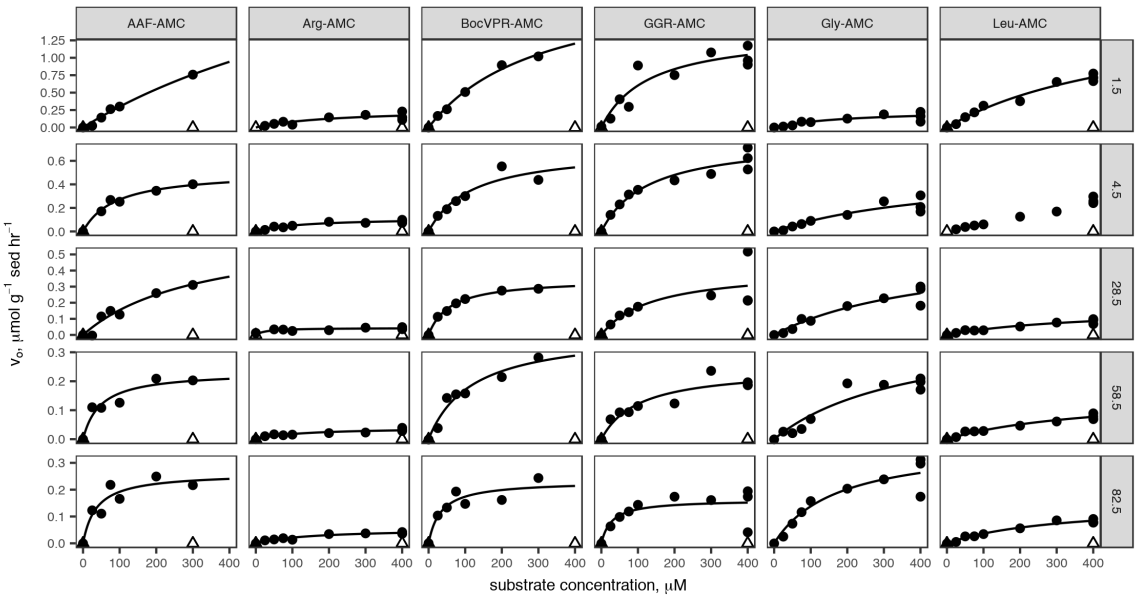

Figure 1: Saturation curves for six substrates measured using the single-cuvette reader methodology at each of six depths. Dark circles indicate "live" samples, open triangles indicate autoclaved controls. Dark lines indicate nonlinear least-squares fits to the Michaelis-Menten rate law. Substrate abbreviations are given in the column headings and are defined in Table 1. Sediment depths are listed on row headings in centimeters below sediment-water interface.

the hydrolysis of eleven different substrates, which may be hydrolyzed by structurally and genetically diverse extracellular peptidases.

Results

PEPTIDASE KINETICS

Combining data from all three sampling dates, unambiguous hydrolysis of eleven different peptidase substrates was observed. All peptidase substrates assayed with the more-sensitive single-cuvette methodology were hydrolyzed much faster in untreated sediments than in autoclaved controls. Kinetics of substrate hydrolysis were qualitatively consistent with the Michaelis-Menten rate law, $v_0 = \frac{V_{max} \times [S]}{K_m + [S]}$ (Fig 1). Estimated V_{max} values ranged from 40 to 3400 nmol g^{-1} sediment hr^{-1} (median 310, interquartile range

190 to 560 nmol g^{-1} sediment hr^{-1}). Throughout the core, AAF-AMC, GGR-AMC, and Gly-AMC were hydrolyzed the fastest, and Arg-AMC was hydrolyzed slowest (Fig S1). Summed V_{max} values decreased with depth from 9.09 µmol AMC g^{-1} sed hr^{-1} at the surface to 1.24 µmol AMC g^{-1} sed hr^{-1}, or 13% of the surface value, at 82.5 cmbsf. Estimated K_m values ranged from 36.1 µM to 1310 µM (median 138 µM, interquartile range 102 to 326 µM), and trended downward (i.e., to greater substrate affinity) with increasing depth (Fig 2). K_m values for hydrolysis of Leu-AMC were the greatest (i.e., lowest substrate affinity) while K_m values for hydrolysis of BocVPR-AMC, GGR-AMC, and Arg-AMC were the least.

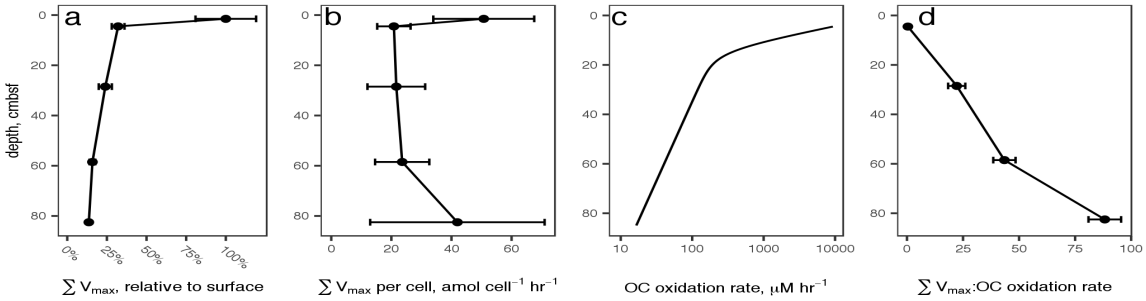

Figure 2: A: The sum of all peptidase V_{max} values, relative to the value at 4.5 cm, versus sediment depth. Error bars represent propagated error of the estimate of V_{max} for each substrate. B: Summed V_{max} relative to cell count. Error bars represent propagated error from summed Vmax and cell counts, and is dominated by cell count uncertainty. C: Organic carbon oxidation rates modeled from sulfate and methane profiles. D: Summed V_{max} relative to modeled carbon oxidation rates. Error bars represent error in summed V_{max} relative to organic carbon oxidation rates, for which uncertainty was not modeled.

In a separate core, hydrolysis rates of D-Phe-AMC, L-Phe-AMC, and L-Orn-AMC were assessed. These were measured using a plate-reader technique that proved insufficiently precise to accurately measure V_{max} or K_m, so we have only reported v_0, which was measured at a high substrate concentration (400 µM) and therefore

approximates V_{max}. Ratios of v_0 for D-Phe-AMC : L-Phe-AMC hydrolysis and L-Orn-AMC : L-Phe-AMC hydrolysis rates increased approximately linearly downcore (Fig 3).

MICROBIAL ABUNDANCE, CELL-SPECIFIC PEPTIDASE ACTIVITY, AND ORGANIC CARBON OXIDATION RATES

Concordantly with potential activities, cell counts decreased more-or-less steadily downcore from 4.5×10^8 cells ml^{-1} wet sediment at 1.5 cmbsf to 7.4×10^7 cells ml^{-1} wet sediment at 82.5 cmbsf. Consequently, cell-specific total potential peptidase activity was roughly constant at 32 +/- 14 amol AMC $cell^{-1}$ hr^{-1} (Fig 2b) with no significant trend as a function of depth. Most of the error in cell-specific peptidase activities results from variance in cell counts rather than in V_{max} estimations.

Organic carbon oxidation rates were estimated using a 2-G model driven by porewater methane and sulfate concentrations. The total organic carbon oxidation rate at 82.5 cmbsf was approximately 0.17% relative to that at 4.5 cmbsf (the top of the model domain), a decrease of almost 3 orders of magnitude (Fig 2c). Thus, summed V_{max} relative to G increased more than 200-fold in the deepest sediments relative to surface sediments.

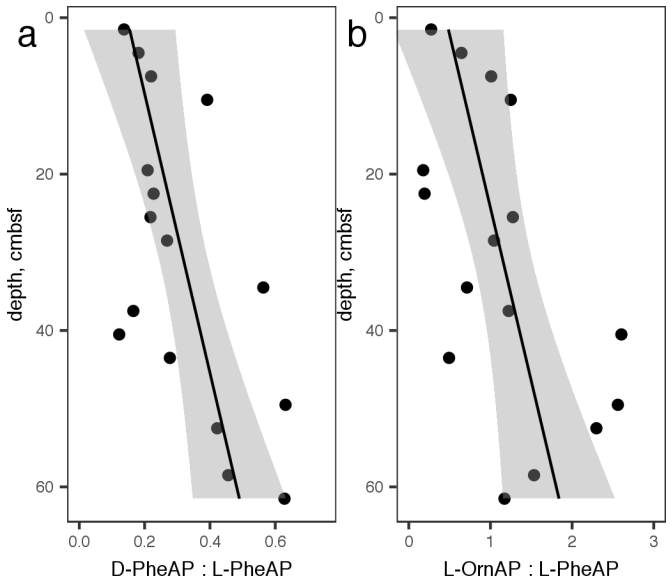

Figure 3: a.) Ratio of v_0 for D-phenylalanine aminopeptidase: L-phenylalanine aminopeptidase and b.) L-ornithine aminopeptidase : L-phenylalanine aminopeptidase.

PEPTIDASE GENES

Samples for genomic analysis were taken from three broad sedimentary zones: the sulfate reduction zone (SRZ, 8-12 cmbsf), sulfate-methane transition zone (SMTZ, two distinct samples from nearby locations, 24-32 cmbsf and 26-30 cmbsf), and the methane-rich zone (52-54 cmbsf; data originally published in Baker *et al.*, 2015). A total of 3739 genes encoding extracellular peptidases were identified among metagenomes from the three depth zones examined, including 685 from SRZ, 1994 from SMTZ, and 1060 from MRZ. Of the genes encoding for peptidases, 0-71% (depending on class of peptidase, algorithm and sediment depth) contained a signal peptide and are likely secreted by the SEC-dependent transport system (supplementary data). Among the genes associated with signal peptides, members of peptidase family C25, belonging to the gingipain family, were by far the most abundant at all depths, accounting for 41-45% of all SP-associated peptidases (Fig. 4). Genes annotated as encoding extracellular methionine aminopeptidases and zinc carboxypeptidases were also abundant (13%-19%). Together, these peptidase classes accounted for 73%, 76%, and 73% of exported peptidases in the SRZ, SMTZ, and MRZ respectively. The composition of protein families was generally consistent with depth,

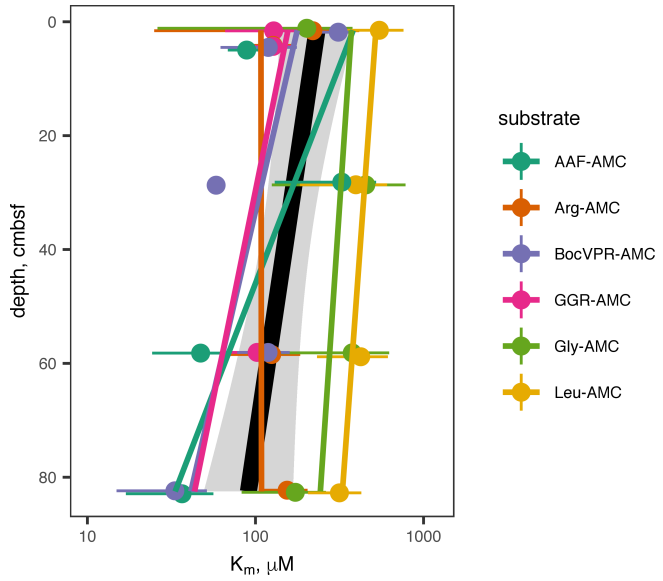

Figure 4: K_m values of extracellular peptidases as a function of depth. Details of substrates and the peptidases they correspond to are in Table 1.

182 particularly among the more-abundant peptidases. Five peptidase annotations were an
183 exception to this trend: peptidase family M1, peptidase family M20/M25/M40, peptidase
184 family M3, M61 glycyl aminopeptidase, and thermophilic metalloprotease (M29) were
185 found in much lower abundance at the SMTZ than the MRZ or SRZ. Given that those
186 correspond to differences of one or a few total reads, these are well within the range of
187 noise.

188 Discussion

189 IDENTITIES OF EXTRACELLULAR PEPTIDASES PRESENT IN WHITE OAK RIVER
190 ESTUARY SEDIMENTS

191 Kinetics of fluorogenic substrate hydrolysis was consistent with the Michaelis-Menten rate law and hydrolysis rates were dramatically slower in autoclaved controls than in "live" treatments, indicating that the substrates were hydrolyzed by enzymes rather than by abiotic factors. The enzyme substrates used here encompassed a diverse range of amino acid and peptide chemistries, including polar and non-polar R groups at the P1 site (i.e., the amino

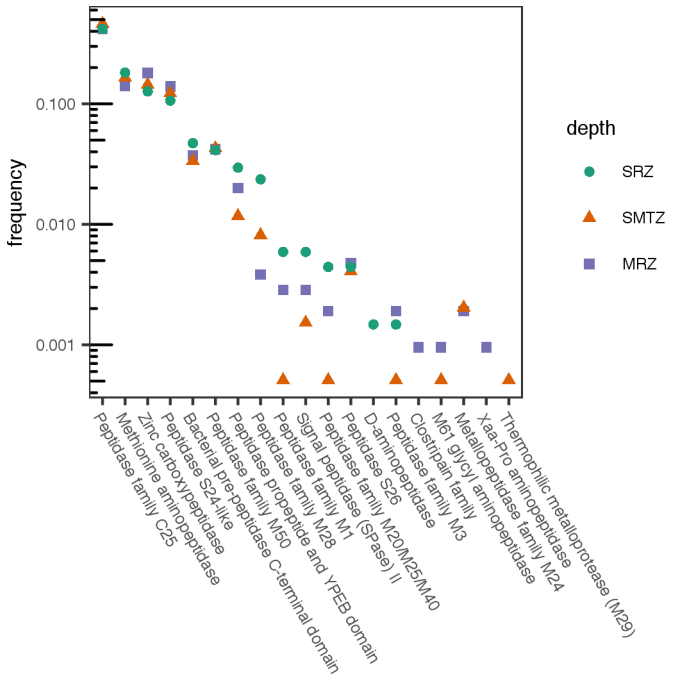

Figure 5: Exported peptidases identified in WOR sediments. Depths SRZ, SMTZ, and MRZ correspond to the sulfate-reducing zone (8-12 cmbsf), sulfate-methane transition zone (24-32 cmbsf) and methane-rich zone (52-54 cmbsf), respectively.

203 acid N-terminal to the scissile bond) and substrates with and without steric protecting
204 groups, which must have been hydrolyzed by endopeptidases (which cleave proteins from
205 within) and aminopeptidases (which cleave proteins from the N terminus) respectively.
206 Peptide bonds adjacent to a diverse set of amino acid residues were cleaved, including
207 glycine (the smallest amino acid), phenylalanine (among the largest amino acids),
208 arginine (positively charged at porewater pH) and leucine (uncharged, hydrophobic),
209 consistent with the presence of a diverse range of extracellular peptidases throughout the
210 core.

211 The metagenomic results also indicated the potential for a diverse range of
212 secreted peptidases, produced by a broad range of taxa, throughout the sediment column.
213 The metagenomic results represent a minimum estimate for the genomic potential for
214 extracellular peptidase production, because they rely on the assumption that only those
215 peptidases associated with signal peptides (SPs) are secreted. Non-SP-based enzyme
216 secretion pathways may also contribute to the pool of extracellular enzymes, including
217 Sec-independent secretion systems (Bendtsen *et al.*, 2005) and release of internal
218 enzymes into the extracellular medium by viral lysis (Danovaro *et al.*, 2008; Breitbart *et*
219 *al.*, 2004).

220 The dominance of genes for exported gingipain-like endopeptidases (class C25) at
221 all depths is consistent with rapid hydrolysis rates of fluorogenic substrates for
222 endopeptidases. Gingipains are endopeptidases with preference for arginine at the P1
223 position (i.e., the N-terminal side of the hydrolyzed bond), which would be active
224 towards the substrates GGR-AMC and Boc-VPR-AMC. Those were among the fastest-

225 hydrolyzed substrates at each depth (Fig. 1), indicating that genes for C25 peptidases
226 were likely expressed. Previously, gingipains have been identified in Thermoprofundales
227 (formerly Marine Benthic Group D) and in Bathyarchaeota, and appear to be widespread
228 in marine sediments (Zhou *et al.*, 2018a; Lloyd *et al.*, 2013b; Orsi *et al.*, 2018). The M28
229 family, also among the most abundant annotations, contains a diverse range of
230 aminopeptidases and carboxypeptidases including leucine aminopeptidase, consistent
231 with the observed hydrolysis of Leu-AMC (Rawlings *et al.*, 2018). Genes for D-
232 aminopeptidases genes were observed, consistent with hydrolysis of D-Phe-AMC.
233 Other abundant genes were annotated as methionine aminopeptidase, zinc
234 carboxypeptidase, a C-terminal domain from bacterial pre-peptidases, and peptidases
235 from the MEROPS families M24, S24, M50, and M28. Potential activities of these
236 peptidases were not assayed. Zinc carboxypeptidases (M20) cleave enzymes from the
237 carboxy-terminus and have strong specificity for Gly at the P1 position (i.e., the position
238 C-terminal to the scissile bond), but little preference for the residue at the P1' position
239 (the position C-terminal to the scissile bond; in a carboxypeptidase this would be the C-
240 terminus of the protein). Methioine aminopeptidases (M24) are metallopeptidases with
241 preference for glycine at the P1 position.
242 S24 and M50 peptidases are less likely to be directly relevant to organic matter
243 processing. S24 peptidases are involved in the SOS response for single-stranded DNA
244 repair (Rawlings *et al.*, 2018). M50 peptidases are membrane-bound enzymes that act as
245 sporulation factors in Bacillus subtilis, and possibly other Bacteria (Green and Cutting,
246 2000; Feng *et al.*, 2007), and which are not secreted. However, DNA repair (Orsi *et al.*,

247 2013; Bird *et al.*) and spore formation (O'Sullivan *et al.*, 2015; Lomstein *et al.*, 2012)
248 both appear to be important survival mechanisms for microorganisms in subsurface
249 sediments. The bacterial C-terminal pre-peptidase domain is often found in secreted
250 peptidases, but is removed prior the peptidase becoming active, and could be associated
251 with a wide range of peptidases (Yeats *et al.*, 2003).

252 Each of these annotations is plausible in terms of what is known about peptidase
253 activities in sediments, and the annotations and observed activities generally agreed with
254 each other. We did not assay for carboxypeptidases (e.g. MEROPS family M20) or
255 methionine aminopeptidase, but carboxypeptidases have previously been observed to be
256 active in estuarine sediments (Pantoja *et al.*, 1997) and the generally broad substrate
257 specificities of extracellular aminopeptidases suggests that methionine aminopeptidases
258 could have contributed to the hydrolysis of the other aminopeptidase substrates (Steen *et*
259 *al.*, 2015). However, a note of caution is also warranted when interpreting peptidase
260 annotations from deeply branching microorganisms: the high diversity of hydrolases
261 makes precise annotations difficult, and the exact substrate specificities of the peptidases
262 in these samples may differ somewhat from those inferred from the annotations
263 (Michalska *et al.*, 2015). Thus, while these annotations are environmentally plausible and
264 generally consistent with the fluorogenic enzyme assays, they should nevertheless be
265 viewed with some skepticism.

PEPTIDASE KINETICS SUGGEST ADAPTAION OF SUBSURFACE PEPTIDASES TO DEGRADED ORGANIC MATTER

Heterotrophic microorganisms in subsurface sediments have little access to fresh organic matter. In the cores described here, which represented ~275 years of sediment deposition, organic matter reactivity decreased by at least three orders of magnitude between the surface and 82.5 cmbsf (Fig 2c). It is challenging to determine what fraction of high- vs low-molecular weight organic matter subsurface microorganisms metabolize. However, the fact that cell-specific V_{max} was more-or-less constant downcore (Fig 2b) suggests that the heterotrophic community relied on complex organic matter to a similar degree at all depths. The cell-specific V_{max} values for Leu-AMC hydrolysis, 21-51 amol cell^{-1} hr^{-1}, are comparable to previous measurements in active environments such as surface sediments (2-100 amol cell^{-1} hr^{-1}) and seawater (mostly less than 100 amol cell^{-1} hr^{-1}, but with some measurements up to 10 nmol cell^{-1} hr^{-1}; Vetter and Deming, 1994 and references therein), consistent with communities that relied primarily on organic carbon derived from macromolecules.

The ratio of ΣV_{max} : OC oxidation rate is sensitive to the mix of enzymes included in the sum, and to the substrate specificity of enzymes assayed (some enzymes will be capable of hydrolyzing multiple substrates). The absolute value of that sum, therefore, is not particularly meaningful. The trend, however, is informative: as sediment depth increased, the potential activity of extracellular peptidases decreased much more slowly than the actual rate of organic carbon oxidation, so the ratio of ΣV_{max} : OC oxidation rate increased dramatically (Fig 2d). V_{max} is a proxy for enzyme concentration, so the

288 observed increase in ΣV_{max} : OC oxidation rate combined with the trend in cell-specific
289 ΣV_{max} suggests that deeper heterotrophic communities exhibited similar demand for
290 detrital OM, but that those enzymes returned bioavailable hydrolysate at a much slower
291 rate because substrate concentrations were lower.

292 The White Oak River subsurface communities were similar to their surface
293 counterparts in terms of reliance on extracellular enzymes for bioavailable organic
294 carbon, although subsurface metabolisms were considerably slower. However, enzyme
295 kinetics and potential activities of D-phenylalanine aminopeptidase, L-phenylalanine
296 aminopeptidase, and L-ornithine aminopeptidase all suggested microbial community
297 adaptation to old, degraded organic matter in deeper sediments.

298 Most amino acids are biosynthesized as L-stereoisomers. As organic matter ages,
299 the ratio of D-amino acids to L-amino acids (D:L ratio) increases with depth, due to
300 abiotic racemization and increased abundance of D-amino acids derived from bacterial
301 cell walls (Bada *et al.*, 1970; Lomstein *et al.*, 2009). Accordingly, the potential activity of
302 D-phenylalanyl aminopeptidase increased relative to that of L-phenylalanyl
303 aminopeptidase, indicating an increased capacity to access degraded organic matter.
304 Ornithine, which is a product of the release of urea from arginine, is another marker for
305 degraded organic matter, while phenylalanine is more characteristic of fresher organic
306 matter (Dauwe *et al.*, 1999), and the relative potential activity of L-phenylalanine
307 aminopeptidase : ornithine aminopeptidase followed the same increasing trend with
308 depth. Finally, the decrease of K_m values with increasing depth indicates peptidases that
309 function more efficiently at lower substrate concentrations. It is intuitive that the

concentration of enzyme-labile organic matter concentrations would decrease downcore, and the observed increase in ΣV_{max} : OC oxidation rate provides direct evidence of that. Taken together, these three observations provide strong evidence for a subsurface heterotrophic microbial community that is increasingly adapted to persist using degraded organic matter at increasing depth.

This evidence raises the ecological question of *how* selective pressure produces a heterotrophic community adapted to degraded organic matter. Modeling and genomic observations in other sedimentary environments suggest that microbial growth rates are too slow for community adaptation by enhanced growth rates of more successful taxa; rather, communities in deeper sediments consist of taxa that were deposited at the sediment-water interface and died at the slowest rates (Starnawski *et al.*, 2017; Bradley *et al.*, 2018). If those findings can be generalized to environments characterized by recalcitrant organic matter, that poses a question: in which aquatic environments are microorganisms capable gaining reproductive advantage by growing on recalcitrant organic carbon? The studies cited above addressed sites at which sedimentation rates, microbial respiration, and likely cell doubling times were considerably slower than in the sediments described here, so even if growth (as opposed to persistence) on recalcitrant organic carbon is not possible in those environments, it may have been in the White Oak River sediments. Alternately, microbial taxa may gain adaptations to metabolize recalcitrant organic matter in environments where labile organic matter is more abundant and growth rates are higher. This scenario would imply that organisms which primarily metabolize more labile organic matter would gain some selective advantage by also

metabolizing recalcitrant organic matter. Further analysis of the mechanisms by which subsurface heterotrophs access degraded sedimentary organic matter may yield insights into how microorganisms survive in low-energy environments, and into the controls on organic carbon preservation in sediments over geological timescales.

Materials and Methods

STUDY SITE

Samples were collected from Station H in the White Oak River Estuary, 34° 44.490' N, 77° 07.44' W, first described by Gruebel and Martens (1984). The White Oak River Estuary occupies a drowned river valley in the coastal plain of North Carolina. Station H is characterized by salinity in the range of 10 to 28 and water depth on the order of 2 m. The flux of ΣCO_2 across the sediment-water interface was 0.46 ± 0.02 mmol m^{-2} hr^{-1} (measured in May of 1987), primarily due to organic carbon oxidation via sulfate reduction. The sediment accumulation rate averages 0.3 cm yr^{-1} (Kelley et al., 1990). Total organic carbon content is approximately 5%. For this study, push cores of 40-85 cm were collected from Station H by swimmers on May 28, 2013, and October 22, 2014. In 2013, cores were transported to the nearby Institute of Marine Sciences (University of North Carolina) at Morehead City, where they were sectioned and processed for enzyme activities, porewater geochemistry, and cell counts within 6 hours of sample collection. Porewater sulfate in 2013 was depleted by 43.5 cm, and methane peaked at 79.5 cm (Fig. S1). In 2014, cores were transported on the day of sampling to

353 the University of Tennessee, Knoxville, stored at 4 °C, and processed for enzyme
354 activities the following day. Samples for metagenomic analysis were collected separately
355 in October 2010 from three sites (sites 1, 2, and 3, as previously described by Baker et al.,
356 2015), all of which are within 550 m of Station H.

357 ENZYME ASSAYS

358 Enzyme assays were performed using different protocols in 2013 (data presented
359 in Figs 1-3) versus 2014 (data presented in Fig 4). In 2013, enzyme assays were
360 performed according to a protocol similar to the one described in Lloyd et al (2013b).
361 Cores were sectioned into 3 cm intervals. The following intervals were selected for
362 enzyme assays: 0-3 cm, 3-6 cm, 27-30 cm, 57-60 cm, and 81-83 cm. Each section was
363 homogenized, and approximately 0.5 ml wet sediment was transferred into separate 5 ml
364 amber glass serum vials, which had been pre-weighed and preloaded with 4 ml anoxic
365 artificial seawater (Sigma Sea Salts, salinity = 15, pH=7.5) Samples were weighed again
366 to determine the precise mass of wet sediment added, and then an appropriate quantity of
367 20 mM peptidase substrate stock dissolved in DMSO was added, up to 90 μL, for final
368 substrate concentrations of 0, 25, 50, 75, 100, 200, or 300 μM. Substrates are listed in
369 Table 1. Triplicate incubations with 400 μM Arg-AMC, Gly-AMC, Leu-AMC and Gly-
370 Gly-Arg-AMC were also created, but these were omitted for Ala-Ala-Phe-AMC and Boc-
371 Phe-Val-Arg-AMC because the latter two substrates are considerably more expensive.
372 Each serum vial was vortexed, briefly gassed with N_2 to remove oxygen introduced with
373 the sample, and approximately 1.3 ml slurry was immediately removed, transferred to a
374 microcentrifuge tube, and placed on ice to quench the reaction. The precise time of

375 quenching was recorded. This was centrifuged at 10,000 × *g* within approximately 15
376 minutes. The supernatant was transferred to a methacrylate cuvette and fluorescence was
377 measured with a Turner Biosystems TBS-380 fluorescence detector set to UV mode
378 (λ_{ex}=365-395 nm, λ_{em}=465-485 nm). Samples were then incubated at 16 °C,
379 approximately the *in situ* temperature, and the sampling procedure was repeated after
380 approximately 3 hours. The rate of fluorescence production was calculated as the increase
381 in fluorescence for each sample divided by the elapsed time between sample quenching.
382 Killed controls were made using homogenized, autoclaved sediments from 35-45 cmbsf.
383 However, we note that autoclaving does not completely destroy sediment enzymes
384 because sorption to mineral surfaces stabilizes enzyme structure, vastly increasing their
385 ability to maintain a functional conformation at high temperatures (Stursova and
386 Sinsabaugh, 2008; Carter *et al.*, 2007; Schmidt, 2016). We therefore used the autoclaved
387 samples as a qualitative control for the null hypothesis that enzymes were responsible for
388 none of the observed substrate hydrolysis, rather than as a quantitative method to
389 distinguish enzymatic substrate hydrolysis from potential abiotic effects. In some
390 sediments, a large fraction of fluorophore can sorb to particles, requiring a correction to
391 observed fluorescence (Coolen *et al.*, 2002; Coolen and Overmann, 2000), but we
392 observed negligible sorption of fluorophore to the White Oak River sediments.
393 In 2014, enzymes were assayed using a protocol based on the approach of Bell et
394 al (2013), which was designed for soil enzyme assays. In this approach, peptidase
395 substrates were mixed with sediment-buffer slurries in 2-mL wells of a deep-well plate.
396 These plates were periodically centrifuged and 250 µL aliquots of supernatant were

397 transferred into a black 96-well microplate. Fluorescence was read using a BioTek
398 Cytation 3 microplate reader (λ_{ex} = 360 nm, λ_{em} = 440 nm). Results from this method
399 proved considerably noisier than the single-cuvette method used in 2013, so kinetic
400 parameters (V_{max} and K_m) were not calculated for these data. Nevertheless, results were
401 qualitatively similar to those from 2013, and we have reported V_{max} from 2014 as v_0
402 measured at 400 μM substrate concentration, which was saturating. In June 2014, the
403 following substrates were assayed: AAF-AMC, Arg-AMC, Boc-VPR-AMC, D-Phe-
404 AMC, Gly-AMC, Leu-AMC, L-Phe-AMC, Orn-AMC, Z-Phe-Arg-AMC, and Z-Phe-Val-
405 Arg-AMC. In October 2014, L-Phe-AMC, D-Phe-AMC, and Orn-AMC were assayed
406 according to the same protocol in 3-cm core sections at 1.5, 4.5, 7.5, 10.5, 19.5, 22.5,
407 25.5, 28.5, 34.5, 37.5, 40.5, 43.5, 49.5, 52.5, 58.5, and 61.5 cmbsf.
408 Peptidase kinetic data were analyzed using R. All raw data and scripts related to
409 enzyme analysis are posted at http://github.com/adsteen/WOR_enz_2013_2014. For
410 samples taken using the more sensitive single-cuvette method, Michaelis-Menten
411 parameters were estimated from nonlinear least squares fits to kinetic data. In the case of
412 Leu-AMC at 4.5 centimeters below seafloor, kinetic data could not successfully be fit to a
413 Michaelis-Menten function, so no K_m was reported and the value of v_0 at the highest
414 substrate concentration was substituted for V_{max}. For analysis of correlations, data sets
415 were qualitatively evaluated for homoskedasticity and normality of residuals using q-q
416 plots and plots of residuals vs fitted values. When untransformed data met those criteria,
417 the null hypothesis of no correlation was tested using linear least-squares regressions.
418 When untransformed data failed to meet those criteria, data were first log-transformed. In

cases in which log-transformed data were wither heteroskedastic or residuals were non-normally distributed, data were rank-transformed and correlations were tested using Spearman's ρ.

GEOCHEMICAL AND MICROBIOLOGICAL MEASUREMENTS

Sediment porosity was measured by mass after drying at 80 °C, according to the equation

$$\phi = \frac{m_w/\rho_w}{m_w/\rho_w + \frac{m_d - S \times m_w/1000}{\rho_{ds}}}$$

Here, m_w represents mass lost after drying, ρ_w represents the density of pure water, m_d represents the mass of the dry sediment, S represents salinity in g kg^{-1}, and ρ_{ds} represents the density of dry sediment (assumed to be 2.5 g cm^{-3}). Porewater sulfate concentrations were measured using a Dionex Ion Chromatograph (Sunnyvale, CA) in porewater that was separated by centrifugation in 15 ml centrifuge tubes at 5000 × *g* for 5 minutes, filtered at 0.2 µm, and acidified with 10% HCl. Methane was measured using 3 ml sediment subsamples that were collected from a cutoff syringe, entering through the side of a core section, immediately after core extrusion. Subsamples were deposited immediately in a 20 ml serum vial containing 1 ml, 0.1 M KOH. These were immediately stoppered and shaken to mix sediment with KOH. Methane was later measured by injecting 500 µl of bottle headspace into a GC-FID (Agilent, Santa Clara, CA) using a headspace equilibrium method (Lapham *et al.*, 2008).

GEOCHEMICAL MODELING

Organic carbon remineralization rates as a function of depth were estimated by applying a multi-component reaction-transport model to depth distributions of sulfate and methane concentration. The model is based on equations described in Boudreau (Boudreau, 1996) and includes only sulfate reduction and methane production due to lack of data regarding oxic and suboxic processes. Thus, the model is limited to depths greater than 4.5 cm where sulfate reduction and methane production are the dominant processes, and bioirrigation and bioturbation may be assumed to be negligible. The organic matter remineralization rate is parameterized using the multi-*G* model first proposed by Jørgensen (1978); a two-component model was sufficient to accurately simulate the sulfate and methane data. For solutes, the upper boundary conditions were measured values at 4.5 cm while the lower boundary conditions (200 cm) were set to zero-gradient. The flux of reactive organic carbon to 4.5 cm was calculated from the sulfate flux across the 4.5 cm horizon and an estimate of methane burial below the lower boundary (the methane flux at the upper boundary was observed to be zero), with an assumed oxidation state of reactive carbon of -0.7. The model contains four adjustable parameters that are set to capture the major details of measured sulfate and methane data: first-order rate constants for both fractions of the reactive carbon pool; the partitioning factor for both fractions, and the rate constant for methane oxidation.

CELL ENUMERATION

Cells were enumerated by direct microscopic counts. One mL of sediment was placed in a 2-mL screw-cap tube with 500 µl of 3% paraformaldehyde in phosphate

461 buffered saline (PBS), in which it was incubated overnight before being centrifuged for 5
462 minutes at 3000 × *g*. The supernatant was removed and replaced with 500 µl of PBS,
463 vortexed briefly and centrifuged again at 3000 × *g*. The supernatant was subsequently
464 removed and replaced with a 1:1 PBS:ethanol solution. Sediments were then sonicated at
465 20% power for 40 seconds to disaggregates cells from sediments and diluted 40-fold into
466 PBS prior to filtration onto a 0.2 µm polycarbonate filter (Fisher Scientific, Waltham,
467 MA) and mounted onto a slide. Cells were stained with 4',6-diamidino-2-phenylindole
468 (DAPI) and enumerated by direct counts using a Leica Epifluorescence Microscope.

469 METAGENOMIC ANALYSIS

470 To resolve the taxonomic distribution of extracellular peptidases we searched a
471 pre-existing White Oak River *de novo* assembled and binned metagenomic dataset (Table
472 S2; Baker *et al.*, 2015) for genes that were assigned extracellular peptidase functions.
473 These assignments were based on best matches to extracellular peptidases in KEGG,
474 pfam, and NCBI-nr (non-redundant) databases using the IMG annotation pipeline
475 (Markowitz et al., 2014). Genes were additionally screened for signal peptidase motifs
476 using the following programs: PrediSI setting the organism group to gram-negative
477 bacteria (Hiller *et al.*, 2004), PRED-Signal trained on archaea (Bagos *et al.*, 2009), the
478 standalone version of PSORT v.3.0 trained against archaea (Yu *et al.*, 2010), and SignalP
479 4.1 using gram-negative bacteria as the organism group (Petersen *et al.*, 2011). All
480 programs were used with default settings if not stated otherwise. Binned genomes from
481 three different depth zones of White Oak River sediments were examined. The sulfate-
482 rich zone (SRZ) genomes were obtained from sites 2 and 3 core sections 8-12 and 8-10

483 cm, respectively. The sulfate-methane transitions zone (SMTZ) genomes were recovered
484 from site 2 and 3 and depths of 30-32 cm and 24-28 cm. The methane-rich zone (MRZ)
485 was from site 1 and 52-54 cm.
486

Acknowledgements

We thank Michael Piehler for access to his laboratory facilities at the University of North Carolina Institute of Marine Sciences, the captain of the R/V Capricorn for sampling assistance, and Terry Hazen for use of lab equipment at the University of Tennessee. We thank Oliver Jeffers for reminding ADS that science is cool. Funding for KHM was provided by NSF grant DBI-1156644 to Steven W. Wilhelm. Funding for ADS was provided by NSF grant OCE-1431598 and a C-DEBI subaward. This work is C-DEBI Contribution number <<to be determined.>>

Conflict of interest

The authors declare no competing financial interests in relation to the work described.

501 ## References

502 Allison SD. (2005). Cheaters, diffusion and nutrients constrain decomposition by
503 microbial enzymes in spatially structured environments. *Ecol Lett* **8**: 626–635.

504 Arnosti C, Bell C, Moorhead DLL, Sinsabaugh RLL, Steen ADD, Stromberger
505 M, *et al.* (2014). Extracellular enzymes in terrestrial, freshwater, and marine
506 environments: perspectives on system variability and common research needs.
507 *Biogeochemistry* **117**: 5–21.

508 Bada JL, Luyendyk BP, Maynard JB. (1970). Marine sediments: Dating by the
509 racemization of amino acids. *Science (80-)* **170**: 730–732.

510 Bagos PG, Tsirigos KD, Plessas SK, Liakopoulos TD, Hamodrakas SJ. (2009).
511 Prediction of signal peptides in archaea. *Protein Eng Des Sel* **22**: 27–35.

512 Baker BJ, Lazar CS, Teske AP, Dick GJ. (2015). Genomic resolution of linkages
513 in carbon, nitrogen, and sulfur cycling among widespread estuary sediment bacteria.
514 *Microbiome* **3**: 14.

515 Bell CW, Fricks BE, Rocca JD, Steinweg JM, McMahon SK, Wallenstein MD.
516 (2013). High-throughput fluorometric measurement of potential soil extracellular enzyme
517 activities. *J Vis Exp* e50961.

518 Bendtsen JD, Kiemer L, Fausbøll A, Brunak S. (2005). Non-classical protein
519 secretion in bacteria. *BMC Microbiol* **5**: 58.

520 Benner R, Amon RMW. (2015). The size-reactivity continuum of major
521 bioelements in the ocean. *Ann Rev Mar Sci* **7**: 185–205.

522 Benz R, Bauer K. (1988). Permeation of hydrophilic molecules through the outer

membrane of gram-negative bacteria. Review on bacterial porins. *Eur J Biochem* **176**: 1–19.

Biddle JF, Lipp JS, Lever MA, Lloyd KG, Sørensen KB, Anderson R, *et al.* (2006). Heterotrophic Archaea dominate sedimentary subsurface ecosystems off Peru. *Proc Natl Acad Sci U S A* **103**: 3846–51.

Bird JT, Tague E, Zinke L, Schmidt JM, Steen AD, Reese BK, *et al.* Uncultured microbial phyla suggest mechanisms for multi-thousand-year subsistence in Baltic Sea sediments. *MBio*.

Boudreau BP. (1996). A method-of-lines code for carbon and nutrient diagenesis in aquatic sediments. *Comput Geosci* **22**: 479–496.

Bradley JA, Amend JP, LaRowe DE. (2018). Survival of the fewest: Microbial dormancy and maintenance in marine sediments through deep time. *Geobiology*. e-pub ahead of print, doi: 10.1111/gbi.12313.

Breitbart M, Felts B, Kelley S, Mahaffy JM, Nulton J, Salamon P, *et al.* (2004). Diversity and population structure of a near-shore marine-sediment viral community. *Proc R Soc B Biol Sci* **271**: 565–574.

Carter DO, Yellowlees D, Tibbett M. (2007). Autoclaving kills soil microbes yet soil enzymes remain active. *Pedobiologia (Jena)* **51**: 295–299.

Coolen MJL, Cypionka H, Sass AM, Sass H, Overmann J. (2002). Ongoing modification of Mediterranean Pleistocene sapropels mediated by prokaryotes. *Science* **296**: 2407–10.

Coolen MJL, Overmann J. (2000). Functional Exoenzymes as Indicators of

Metabolically Active Bacteria in 124,000-Year-Old Sapropel Layers of the Eastern Mediterranean Sea. *Appl Environ Microbiol* **66**: 2589–2598.

Danovaro R, Dell'Anno A, Corinaldesi C, Magagnini M, Noble R, Tamburini C, *et al.* (2008). Major viral impact on the functioning of benthic deep-sea ecosystems. *Nature* **454**: 1084–1087.

Dauwe B, Middelburg JJ, Herman PMJ, Heip CHR. (1999). Linking diagenetic alteration of amino acids and bulk organic matter reactivity. *Limnol Oceanogr* **44**: 1809–1814.

Feng L, Yan H, Wu Z, Yan N, Wang Z, Jeffrey PD, *et al.* (2007). Structure of a site-2 protease family intramembrane metalloprotease. *Science* **318**: 1608–12.

Green DH, Cutting SM. (2000). Membrane topology of the Bacillus subtilis pro-sigma(K) processing complex. *J Bacteriol* **182**: 278–85.

Gruebel KA, Martens CS. (1984). Radon-222 tracing of sediment-water chemical transport in an estuarine sediment. *Limnol Oceanogr* **29**: 587–597.

Hiller K, Grote A, Scheer M, Münch R, Jahn D. (2004). PrediSi: Prediction of signal peptides and their cleavage positions. *Nucleic Acids Res* **32**. e-pub ahead of print, doi: 10.1093/nar/gkh378.

Hoehler TM, Jørgensen BB. (2013). Microbial life under extreme energy limitation. *Nat Rev Microbiol* **11**: 83–94.

Jacobson Meyers ME, Sylvan JB, Edwards KJ. (2014). Extracellular enzyme activity and microbial diversity measured on seafloor exposed basalts from Loihi seamount indicate the importance of basalts to global biogeochemical cycling. *Appl*

Environ Microbiol **80**: 4854–64.

Jørgensen BB. (1978). A comparison of methods for the quantification of bacterial sulfate reduction in coastal marine sediments: II. Calculation from mathematical models. *Geomicrobiol J* **1**: 29–47.

Jørgensen BB, Marshall IPG. (2016). Slow Microbial Life in the Seabed. *Ann Rev Mar Sci* **8**: 311–32.

Kelley CA, Martens CS, Chanton JPJP. (1990). Variations in sedimentary carbon remineralization rates in the White Oak River estuary, North Carolina. *Limnol Oceanogr* **35**: 372–383.

Kubo K, Lloyd KG, F Biddle J, Amann R, Teske A, Knittel K. (2012). Archaea of the Miscellaneous Crenarchaeotal Group are abundant, diverse and widespread in marine sediments. *ISME J* **6**: 1949–65.

Lapham LL, Chanton JP, Martens CS, Sleeper K, Woolsey JR. (2008). Microbial activity in surficial sediments overlying acoustic wipeout zones at a Gulf of Mexico cold seep. *Geochemistry, Geophys Geosystems* **9**: Q06001.

Lazar CS, Baker BJ, Seitz K, Hyde AS, Dick GJ, Hinrichs K-U, *et al.* (2016). Genomic evidence for distinct carbon substrate preferences and ecological niches of Bathyarchaeota in estuarine sediments. *Environ Microbiol* **18**: 1200–11.

Lloyd KG, Alperin MJ, Teske A. (2011). Environmental evidence for net methane production and oxidation in putative ANaerobic MEthanotrophic (ANME) archaea. *Environ Microbiol* **13**: 2548–2564.

Lloyd KG, Schreiber L, Petersen DG, Kjeldsen KU, Lever MA, Steen AD, *et al.*

589 (2013a). Predominant archaea in marine sediments degrade detrital proteins. *Nature* **496**:
590 215–8.
591 Lloyd KG, Schreiber L, Petersen DG, Kjeldsen KU, Lever MA, Steen AD, *et al.*
592 (2013b). Predominant archaea in marine sediments degrade detrital proteins. *Nature* **496**.
593 e-pub ahead of print, doi: 10.1038/nature12033.
594 Lloyd KG, Steen AD, Ladau J, Yin J, Crosby L. (2018). Phylogenetically Novel
595 Uncultured Microbial Cells Dominate Earth Microbiomes Neufeld JD (ed). *mSystems* **3**:
596 e00055-18.
597 Lomstein BA, Langerhuus AT, D'Hondt S, Jørgensen BB, Spivack AJ. (2012).
598 Endospore abundance, microbial growth and necromass turnover in deep sub-seafloor
599 sediment. *Nature* **484**: 101–4.
600 Lomstein BA, Niggemann J, Jørgensen BB, Langerhuus AT. (2009).
601 Accumulation of prokaryotic remains during organic matter diagenesis in surface
602 sediments off Peru. *Limnology* **54**: 1139–1151.
603 Martens CS, Goldhaber MB. (1978). Early diagenesis in transitional sedimentary
604 environments of the White Oak River Estuary, North Carolina. *Limnol Oceanogr* **23**:
605 428–441.
606 Meng J, Xu J, Qin D, He Y, Xiao X, Wang F. (2014). Genetic and functional
607 properties of uncultivated MCG archaea assessed by metagenome and gene expression
608 analyses. *ISME J* **8**: 650–9.
609 Michalska K, Steen AD, Chhor G, Endres M, Webber AT, Bird J, *et al.* (2015).
610 New aminopeptidase from 'microbial dark matter' archaeon. *FASEB J* **29**: 4071–4079.

611 O'Sullivan LA, Roussel EG, Weightman AJ, Webster G, Hubert CR, Bell E, *et al.*
612 (2015). Survival of Desulfotomaculum spores from estuarine sediments after serial
613 autoclaving and high-temperature exposure. *ISME J* **9**: 922–933.
614 Obayashi Y, Suzuki S. (2005). Proteolytic enzymes in coastal surface seawater:
615 Significant activity of endopeptidases and exopeptidases. *Limnol Oceanogr* **50**: 722–726.
616 Orsi WD, Edgcomb VP, Christman GD, Biddle JF. (2013). Gene expression in
617 the deep biosphere. *Nature* **499**: 205–208.
618 Orsi WD, Richards TA, Francis WR. (2018). Predicted microbial secretomes and
619 their target substrates in marine sediment. *Nat Microbiol* **3**: 32–37.
620 Pantoja S, Lee C, Marecek JF. (1997). Hydrolysis of peptides in seawater and
621 sediment. *Mar Chem* **57**: 25–40.
622 Petersen TN, Brunak S, von Heijne G, Nielsen H. (2011). SignalP 4.0:
623 discriminating signal peptides from transmembrane regions. *Nat Methods* **8**: 785–6.
624 Rawlings ND, Barrett AJ, Thomas PD, Huang X, Bateman A, Finn RD. (2018).
625 The MEROPS database of proteolytic enzymes, their substrates and inhibitors in 2017
626 and a comparison with peptidases in the PANTHER database. *Nucleic Acids Res* **46**:
627 D624–D632.
628 Reintjes G, Arnosti C, Fuchs BM, Amann R. (2017). An alternative
629 polysaccharide uptake mechanism of marine bacteria. *ISME J* **11**: 1640–1650.
630 Schimel JP, Weintraub MN. (2003). The implications of exoenzyme activity on
631 microbial carbon and nitrogen limitation in soil: a theoretical model. *Soil Biol Biochem*
632 **35**: 549–563.

Schmidt J. (2016). Microbial Extracellular Enzymes in Marine Sediments: Methods Development and Potential Activities in the Baltic Sea Deep Biosphere. University of Tennessee - Knoxville.

Starnawski P, Bataillon T, Ettema TJG, Jochum LM, Schreiber L, Chen X, *et al.* (2017). Microbial community assembly and evolution in subseafloor sediment. *Proc Natl Acad Sci U S A* **114**: 2940–2945.

Steen AD, Arnosti C. (2013). Extracellular peptidase and carbohydrate hydrolase activities in an Arctic fjord (Smeerenburgfjord, Svalbard. *Aquat Microb Ecol* **69**: 93–99.

Steen AD, Arnosti C. (2011). Long lifetimes of β-glucosidase, leucine aminopeptidase, and phosphatase in Arctic seawater. *Mar Chem* **123**: 127–132.

Steen AD, Vazin JPJP, Hagen SMSM, Mulligan KHKH, Wilhelm SWSW. (2015). Substrate specificity of aquatic extracellular peptidases assessed by competitive inhibition assays using synthetic substrates. *Aquat Microb Ecol* **75**: 271–281.

Stursova M, Sinsabaugh RL. (2008). Stabilization of oxidative enzymes in desert soil may limit organic matter accumulation. *Soil Biol Biochem* **40**: 550–553.

Vetter YA, Deming JW. (1994). Extracellular enzyme activity in the Arctic Northeast Water polynya. *Mar Ecol Prog Ser* **114**: 23–34.

Vetter YAY, Deming JJW, Jumars PPA, Krieger-Brockett BBB. (1998). A Predictive Model of Bacterial Foraging by Means of Freely Released Extracellular Enzymes. *Microb Ecol* **36**: 75–92.

Yeats C, Bentley S, Bateman A. (2003). New knowledge from old: in silico discovery of novel protein domains in Streptomyces coelicolor. *BMC Microbiol* **3**: 3.

655 Yu NY, Wagner JR, Laird MR, Melli G, Rey S, Lo R, *et al.* (2010). PSORTb 3.0:
656 improved protein subcellular localization prediction with refined localization
657 subcategories and predictive capabilities for all prokaryotes. *Bioinformatics* **26**: 1608–
658 1615.
659 Zhou Z, Liu Y, Lloyd KG, Pan J, Yang Y, Gu J-D, *et al.* (2018a). Genomic and
660 transcriptomic insights into the ecology and metabolism of benthic archaeal
661 cosmopolitan, Thermoprofundales (MBG-D archaea). *ISME J* 1.
662 Zhou Z, Pan J, Wang F, Gu J-D, Li M. (2018b). Bathyarchaeota: globally
663 distributed metabolic generalists in anoxic environments. *FEMS Microbiol Rev* **42**: 639–
664 655.
665
666

667 ## Table

668 Table 1: Substrates used in this study and the enzymes that hydrolyze them. AMC stands
669 for aminomethylcoumarin, the moiety that becomes fluorescent after hydrolysis of the
670 peptide bond. All amino acids are in the L- stereoconformation unless otherwise noted.
671 Enzymes are described as "putative" because the substrate specificity of many
672 environmental peptidases is fairly broad, so multiple peptidases may hydrolyze any given
673 substrate.

Substrate	Abbreviation	Putative enzyme
L-arginine-7-amido-4-methylcoumarin	Arg-AMC	arginyl aminopeptidase
L-glycine-7-amido-4-methylcoumarin	Gly-AMC	glycyl aminopeptidase
L-leucine-7-amido-4-methylcoumarin	Leu-AMC	leucyl aminopeptidase
Carboxybenzoyl-glycine-glycine-arginine-7-amido-4-methylcoumarin	Z-GGR-AMC	gingipain and other endopeptidases
Alanine-alanine-phenylalanine-7-amido-4-methylcoumarine	AAF-AMC	clostripain and other endopeptidases
Boc-valine-proline-arginine-AMC	Boc-VPR-AMC	gingipain and other endopeptidases
D-phenylalanine-AMC	D-Phe-AMC	D-phenyalanine aminopeptidase
L-phenylalanine-AMC	L-Phe-AMC	L-phenylalanine-aminopeptidase
Ornithine-AMC	Orn-AMC	ornithine aminopeptidase

674

675

Figures and Legends

Figure 1: Saturation curves for six substrates measured using the single-cuvette reader methodology at each of six depths. Dark circles indicate "live" samples, open triangles indicate autoclaved controls. Lines indicate nonlinear least-squares fits to the Michaelis-Menten rate law. Substrate abbreviations are given in the column headings and are defined in Table 1. Sediment depths are listed on row headings in centimeters below sediment-water interface.

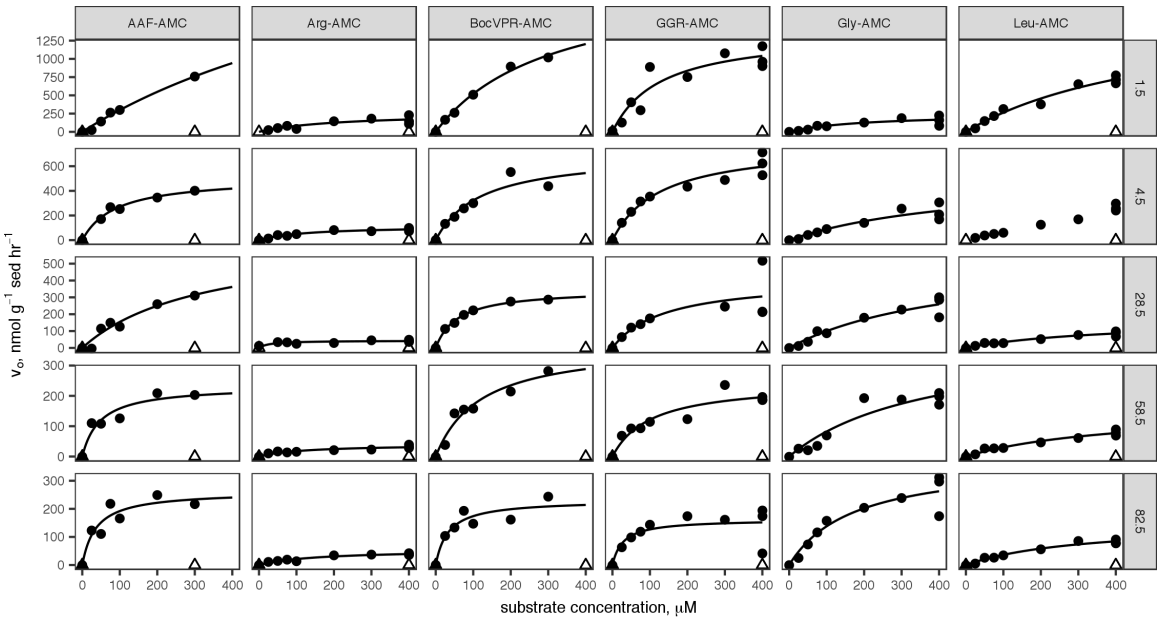

Figure 2: a.) The sum of all peptidase Vmax values, relative to the value at 4.5 cm, versus sediment depth. Error bars represent propagated error of the estimate of V_{max} for each substrate. b.) Summed V_{max} relative to cell count. Error bars represent propagated error from summed Vmax and cell counts, and is dominated by cell count uncertainty. c.) Organic carbon oxidation rates modeled from sulfate and methane profiles. d.) Summed V_{max} relative to modeled carbon oxidation rates. Error bars represent error in summed V_{max} relative to organic carbon oxidation rates, for which uncertainty was not modeled.

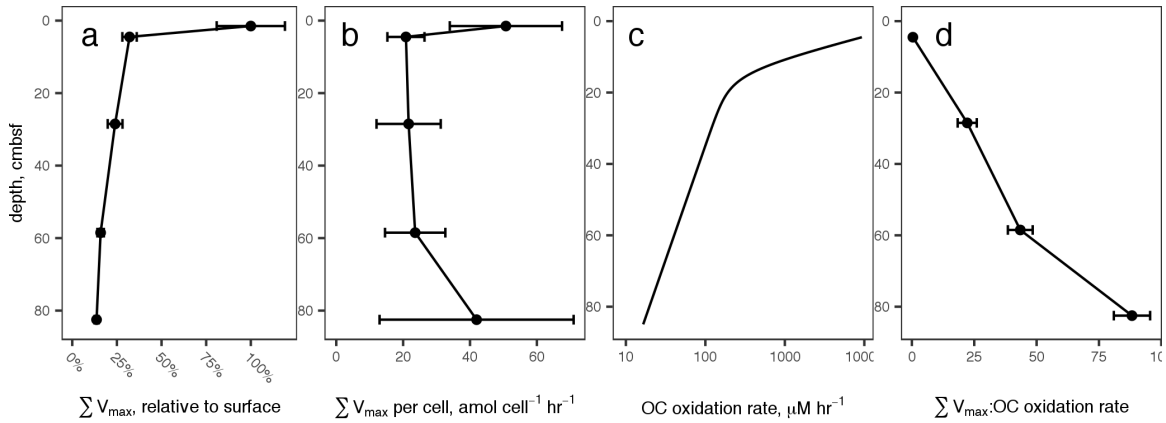

Fig 3: a.) Ratio of v_0 for D-phenylalanine aminopeptidase: L-phenylalanine aminopeptidase and b.) L-ornithine aminopeptidase : L-phenylalanine aminopeptidase.

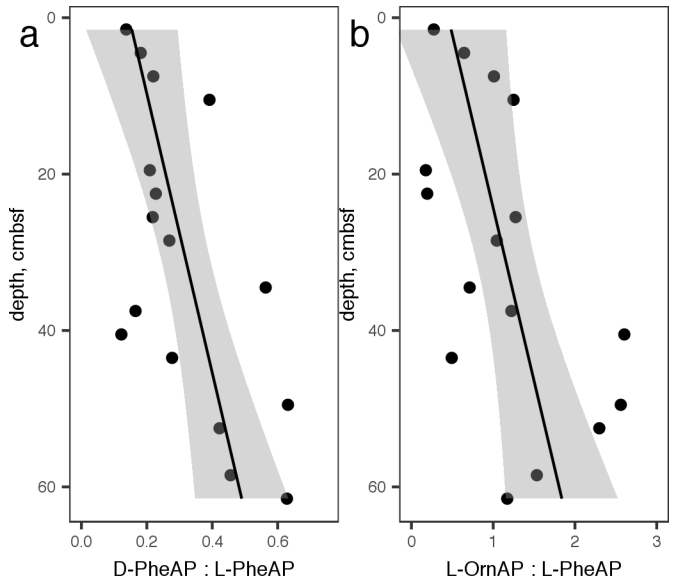

Fig 4: K_m values of extracellular peptidases as a function of depth. Details of substrates and the peptidases they correspond to are in Table 1.

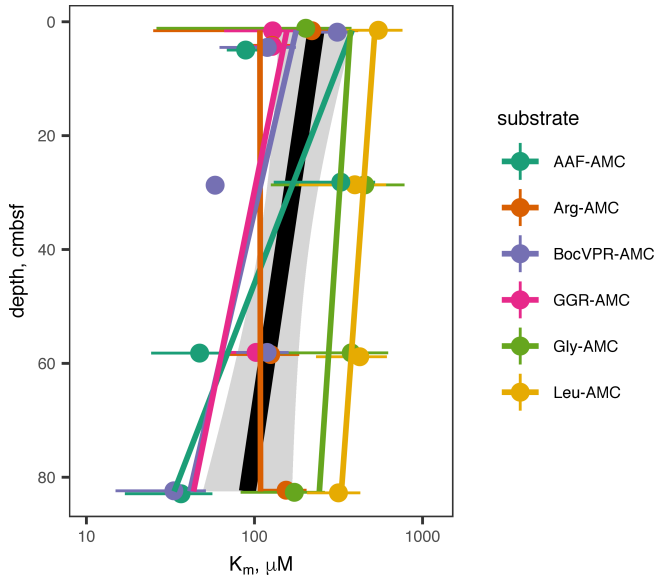

707 Fig 5: Frequency of reads for genes of various classes of extracellular peptidases that
708 were associated with signal peptidases, relative to all genes for extracellular peptidases at
709 that depth. SRZ, SMTZ, and MRZ correspond to “sulfate reducing zone” (8-12 cmbsf),
710 “sulfate-methane transition zone” (24-32 cmbsf) and “methane-rich zone” (24-28 cmbsf)
711 respectively.

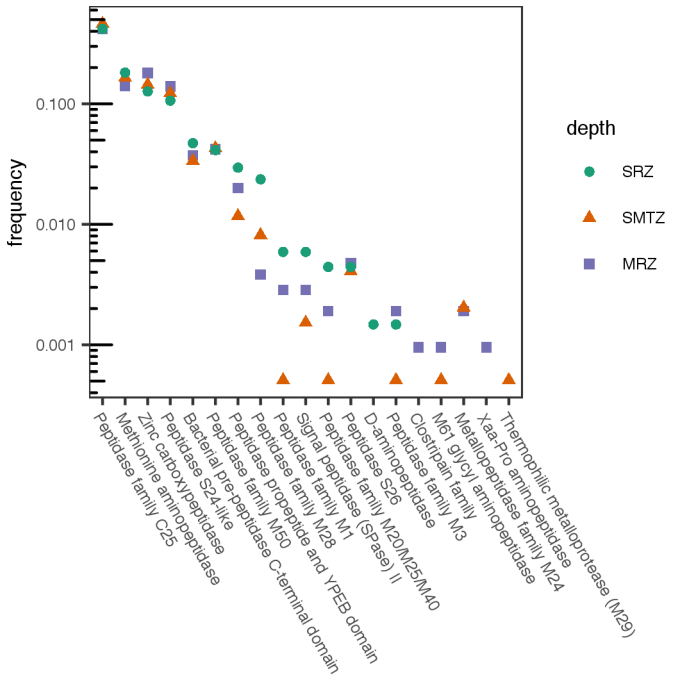

712

713

714

715 **Supplemental Information**

716 Fig S1: V_{max} and K_m values.

717

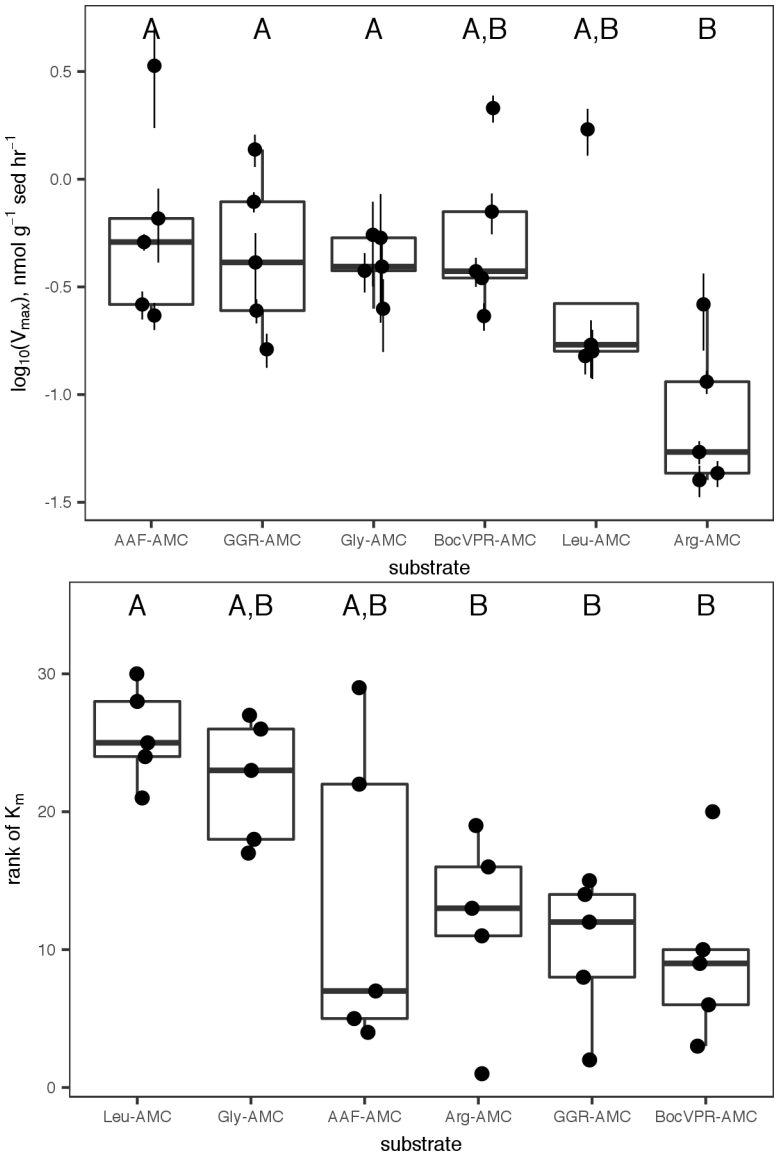

718

719

720 Supplemental file: annotations of all peptidases included in this manuscript.

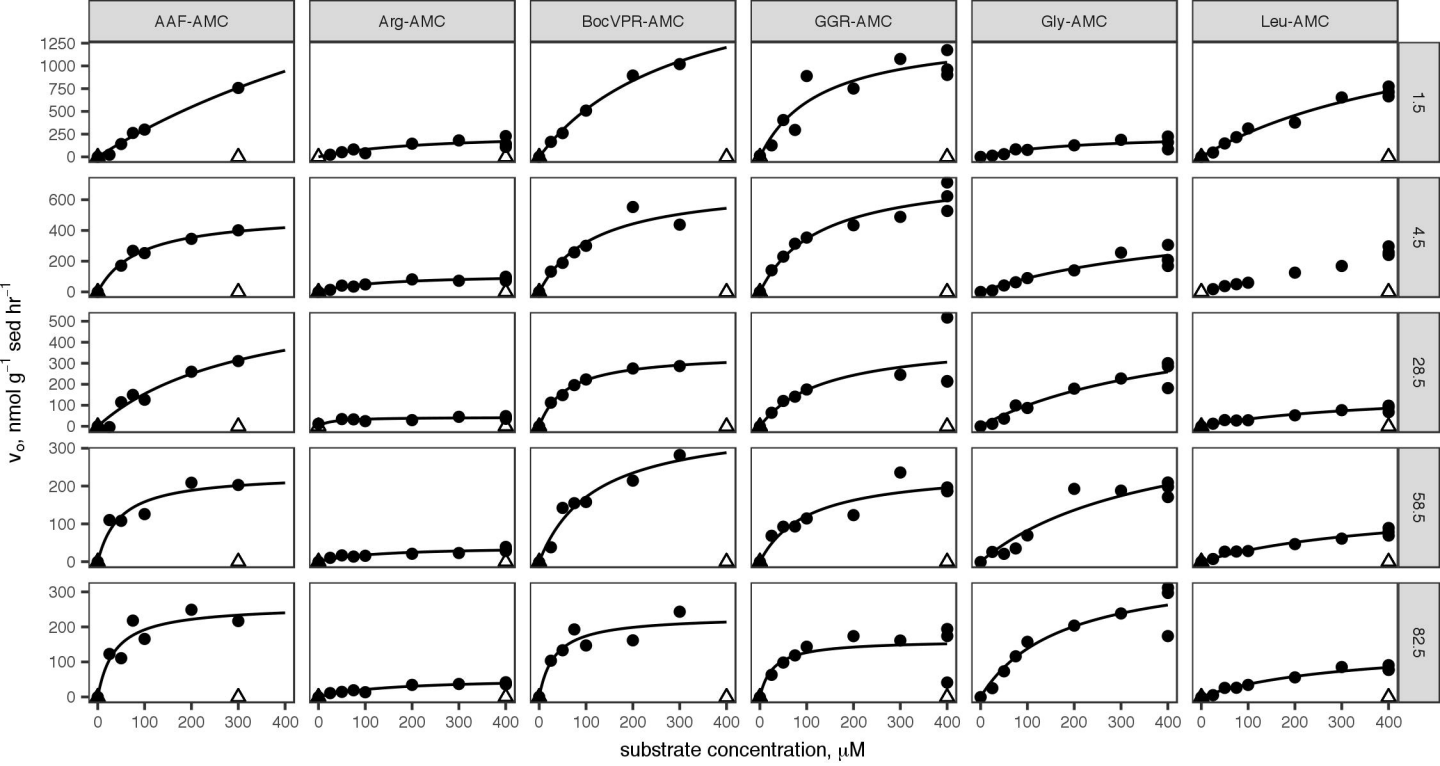
AAF-AMC
Arg-AMC
BocVPR-AMC
GGR-AMC
Gly-AMC
Leu-AMC
1.5
4.5
28.5
58.5
82.5
v_o, nmol g^{-1} sed hr^{-1}
substrate concentration, μM

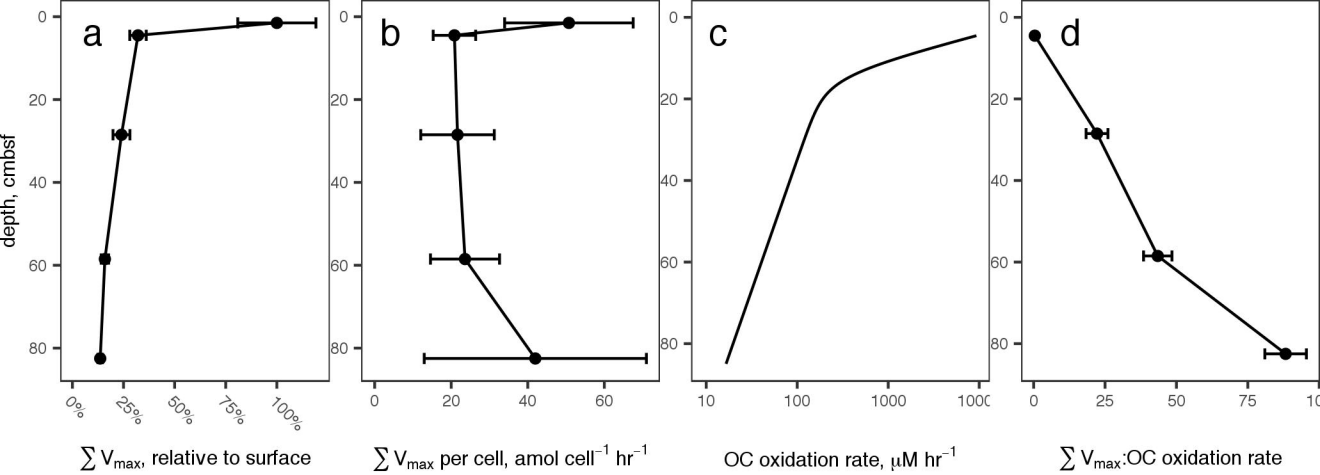
a
b
c
d
depth, cmbsf
0
20
40
60
80
0%
25%
50%
75%
100%
0
20
40
60
10
100
1000
1000
0
25
50
75
∑ Vmax, relative to surface
∑ Vmax per cell, amol cell−1 hr−1
OC oxidation rate, μM hr−1
∑ Vmax:OC oxidation rate

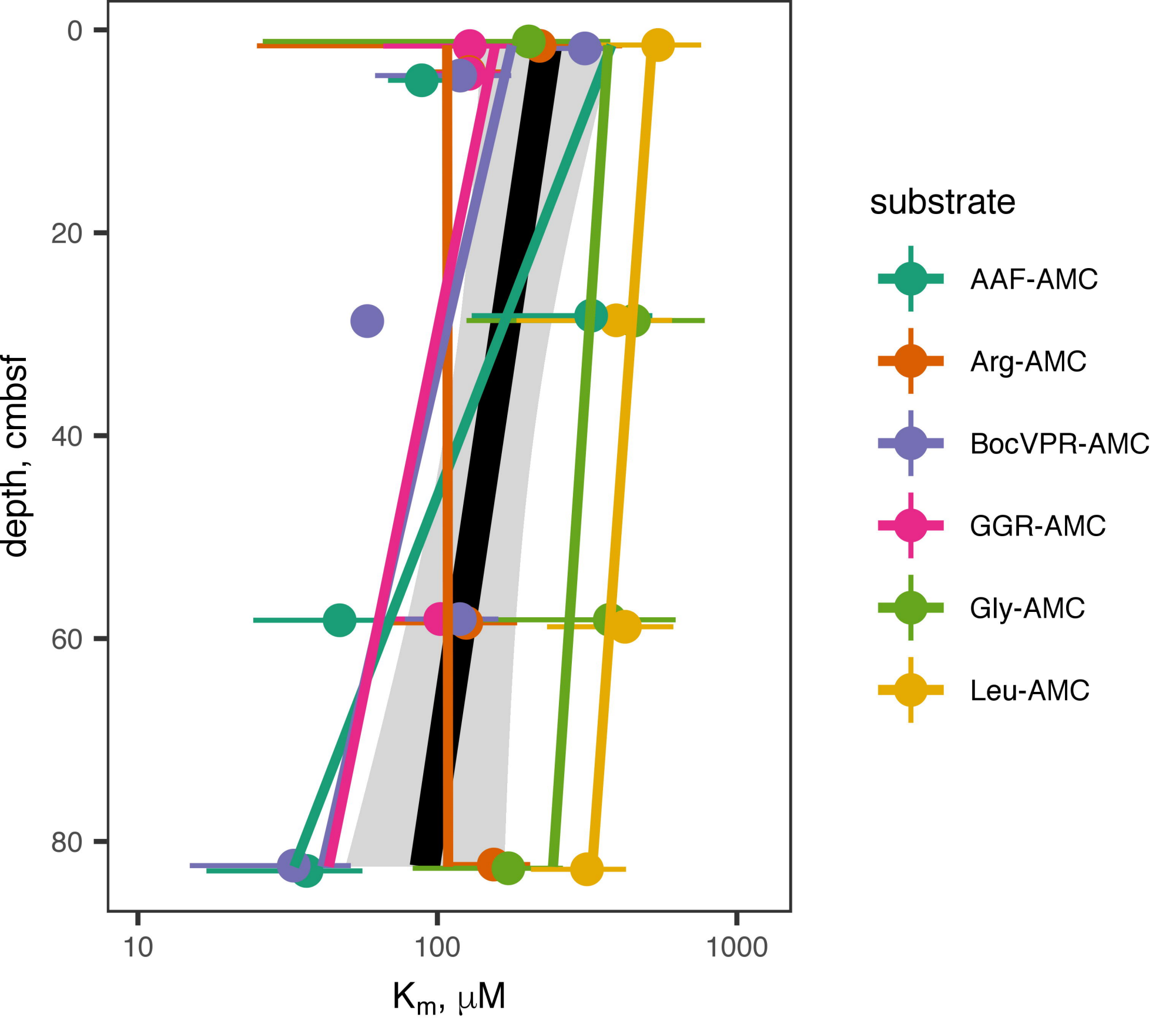
0
20
40
60
80
depth, cmbsf
10
100
1000
K_m, μM
substrate
AAF-AMC
Arg-AMC
BocVPR-AMC
GGR-AMC
Gly-AMC
Leu-AMC

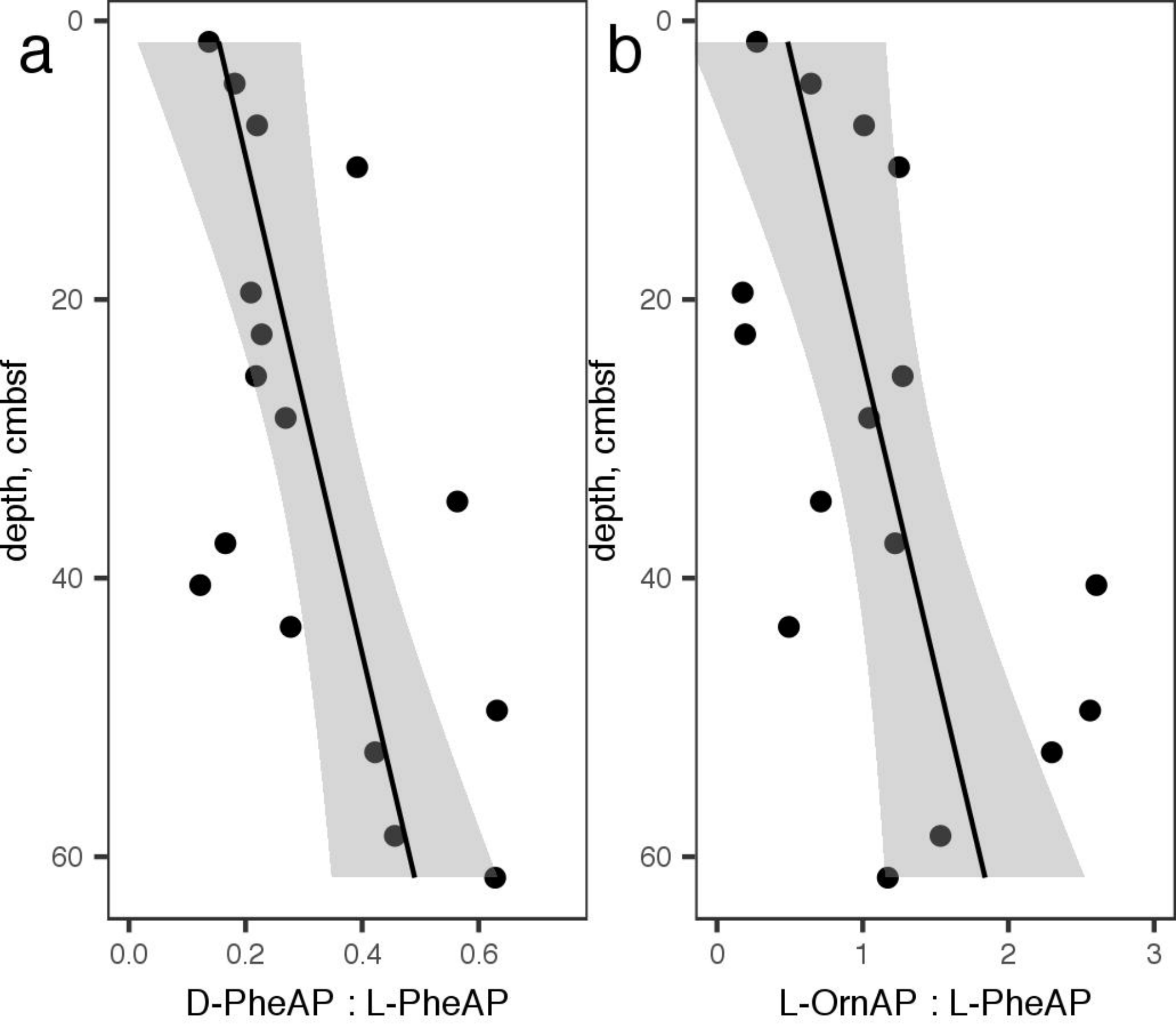
a
b
depth, cmbsf
0
20
40
60
0.0
0.2
0.4
0.6
D-PheAP : L-PheAP
0
1
2
3
L-OrnAP : L-PheAP

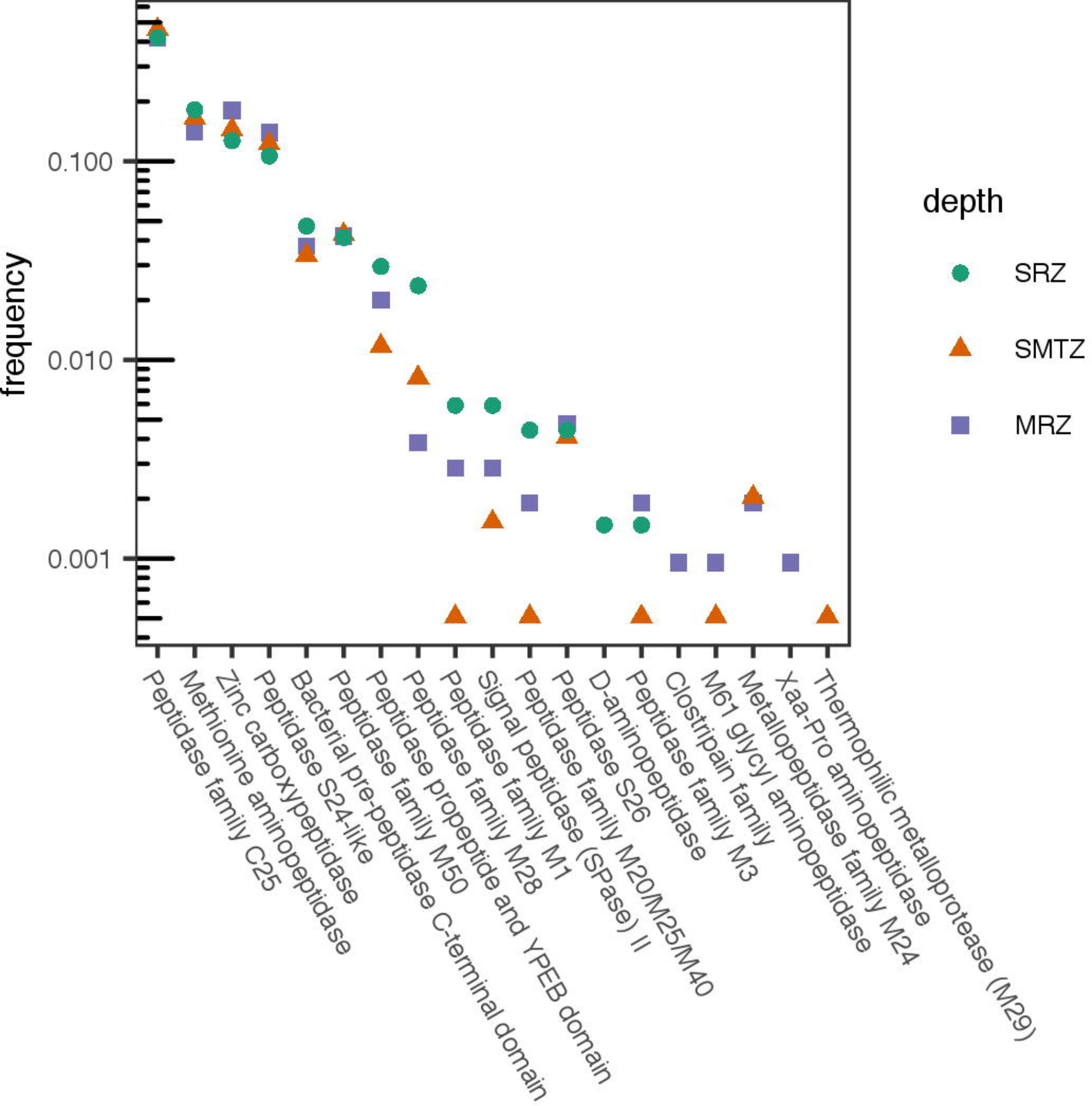
frequency
0.100
0.010
0.001
depth
SRZ
SMTZ
MRZ
Peptidase family C25
Methionine aminopeptidase
Zinc carboxypeptidase
Peptidase S24-like
Bacterial pre-peptidase C-terminal domain
Peptidase family M50
Peptidase propeptide and YPEB domain
Peptidase family M28
Signal peptidase (SPase) II
Peptidase family M1
Peptidase S26
D-aminopeptidase
Peptidase family M20/M25/M40
Clostripain family
M61 glycyl aminopeptidase
Peptidase family M3
Metallopeptidase family M24
Xaa-Pro aminopeptidase
Thermophilic metalloprotease (M29)